11

Countercurrent Flow in a PWR Hot Leg under Reflux Condensation

Noritoshi Minami[1], Michio Murase[2] and Akio Tomiyama[3]
[1]*The Kansai Electric Power Company, Inc.,*
[2]*Institute of Nuclear Safety System, Inc.,*
[3]*Graduate School of Engineering, Kobe University*
Japan

1. Introduction

Nuclear power plants periodically shut down for plant maintenance and refueling. During a pressurized water reactor (PWR) plant outage, decay heat is removed by residual heat removal (RHR) systems. The reactor coolant level temporarily needs to be kept around the middle of the primary loop to inspect the steam generator (SG) tubes and so on. This operation is called "mid-loop operation". In some plants, a loss of RHR event occurred during the mid-loop operation (USNRC, 1987, USNRC, 1990). Probabilistic safety assessment (PSA) studies under plant shutdown conditions have been performed and they confirmed that the loss of RHR cooling during the mid-loop operation is a relatively high risk event for PWR plants. One of the effective methods to cool the reactor core in this event is reflux condensation, in which water condensed in a SG flows into the reactor core through a hot leg and cools down the reactor core as shown in **Fig. 1**. In the reflux condensation, steam generated in the core and water condensed in the SG form a countercurrent flow in the hot leg. This phenomenon limits water into the reactor vessel and affects the performance of core cooling.

System computer codes, as typified by RELAP, employ a simplified model to a certain extent to calculate efficiency, however, the hot leg consists of a horizontal section, elbow, and inclined section. Hence it is unclear whether the countercurrent flow in the hot leg can be well predicted or not. To improve reliability of the transient analysis, we need to understand and model the countercurrent flow in the hot leg.

A number of experiments have been made about the countercurrent flow in the hot leg (Richter et al., 1978, Ohnuki, 1986, Ohnuki et al., 1988, Mayinger et al., 1993, Wongwises, 1996, Navarro, 2005), observations of detailed flow patterns in the hot leg, however, have not been reported. On the other hand, numerical simulations are a realistic way to evaluate the flow, because it is difficult to check the flow pattern in the actual PWR hot leg. Few examples of numerical simulations have been reported, however.

Our objectives in this study were to clarify the flow pattern and dominant factors of the countercurrent flow and to develop the flow model which improves the reliability of the transient analysis. At first, we carried out air-water experiments with a scale model of the actual PWR hot leg. We used two types of small scale PWR hot legs. One was a 1/5th scale

rectangular duct (Minami et al., 2008a), and the other was a 1/15th scale circular pipe (Minami et al., 2010a). Then we carried out numerical simulations of these small scale experiments to investigate flow pattern and CCFL characteristics (Minami et al., 2008b and 2010b). We used a three-dimensional two-fluid model to evaluate the capability of predicting countercurrent flow in the hot leg.

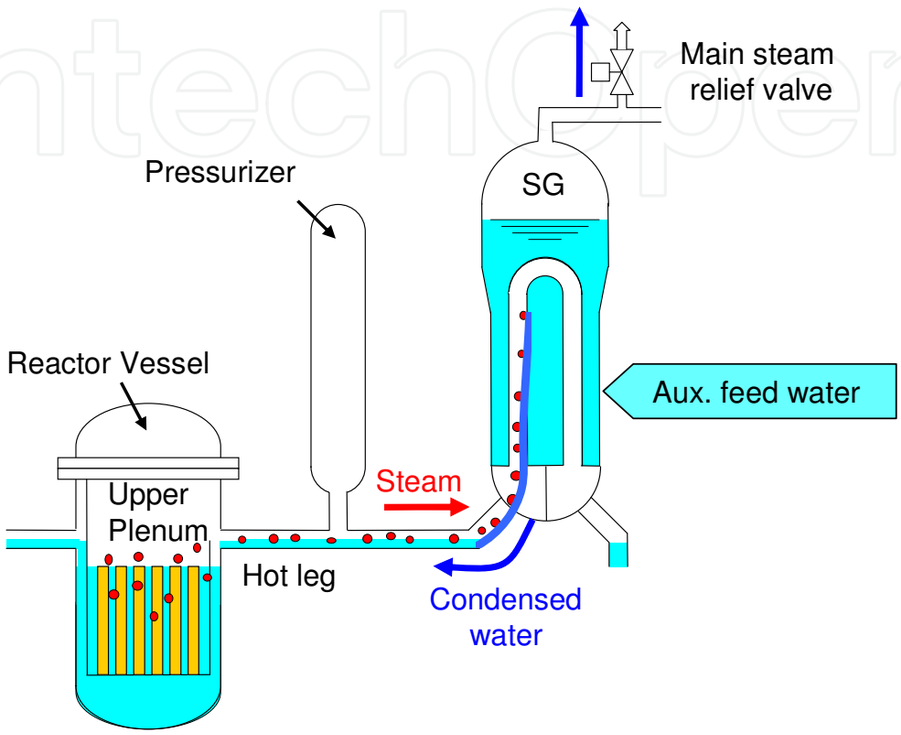

Fig. 1. Schematic view of reflux condensation

2. Experiments

The gas-liquid two-phase flow is complex because the gas-liquid interface takes various geometric configurations and it changes with time. It is, therefore, important to grasp the interfacial behavior. Hence we carried out air-water experiments with a rectangular duct. We chose the rectangular duct because observing the countercurrent flow and following the interface are easy in this duct. Then we carried out experiments with a circular pipe having a configuration geometrically similar to the actual hot leg.

2.1 Experimental setup

Figure 2 shows schematic view of the experimental setup. It consists of the upper tank, which corresponds to the inlet plenum of the SG, the hot leg, the lower tank, which corresponds to the upper plenum of the reactor vessel, the reservoir, and the air and water supply systems. Tap water at room temperature is pumped to the upper tank through a flow meter. Air is supplied from a compressor and flows into the lower tank through a regulator and a flow meter. When CCFL occurs in the hot leg, some of the water overflows the upper tank and drains into the reservoir.

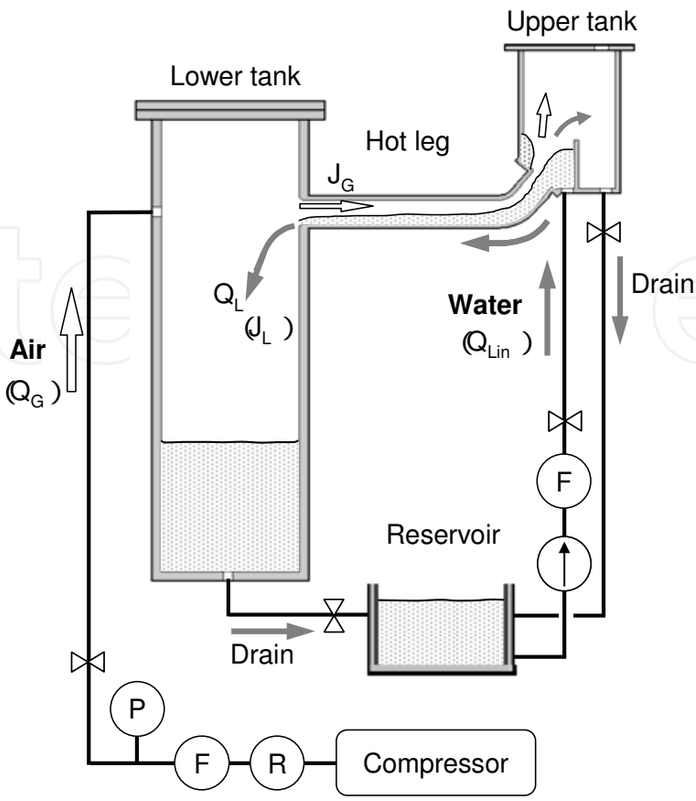

Fig. 2. Schematic view of experimental setup

2.1.1 1/5-scale rectangular duct

Figure 3 shows the test section of the 1/5-scale rectangular duct, which is made of transparent acrylic resin to allow easy observation of countercurrent flow. The height is about 1/5th that of the pipe diameter of an actual PWR hot leg. The inclination of the inclined pipe is 50°.

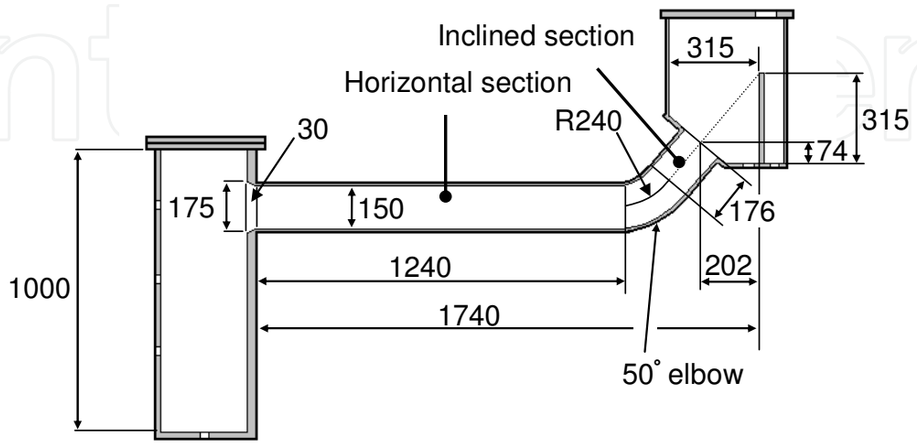

Fig. 3. Test section of 1/5th rectangular duct (unit: mm)

2.1.2 1/15-scale circular pipe

The equipment used is the same as for the rectangular duct setup (Fig. 2). **Figure 4** shows the test section of the 1/15-scale circular pipe. The hot leg consists of the horizontal section, elbow section, inclined section, and is made of transparent acrylic resign. The configuration is geometrically similar to the actual PWR hot leg, while the size is 1/15th. Hence the inner diameter D is 50 mm. The inclination of the inclined pipe is 50°.

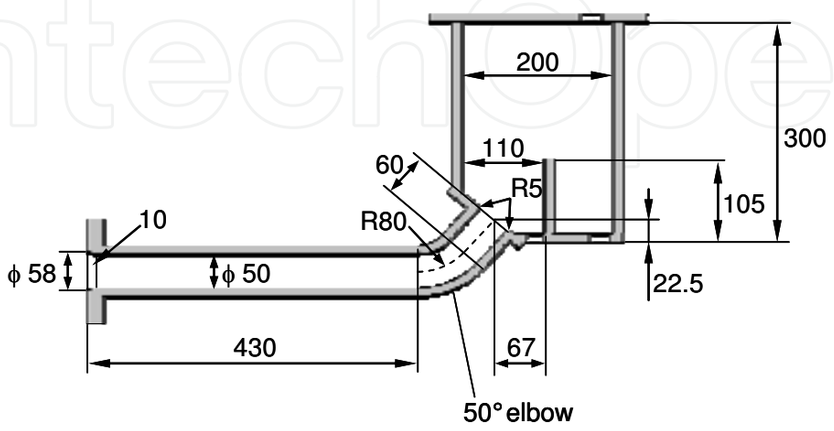

Fig. 4. Test section of 1/15th circular pipe (unit: mm)

2.2 Experimental method

2.2.1 Flow patterns

Observation of flow patterns in the horizontal section, the elbow section, and the inclined section was done by keeping the supplied water flow rate Q_{Lin} constant. The air volumetric flux in the hot leg J_G was gradually increased until water ceased to flow into the lower tank (=Q_L of water flow rate into the lower tank equal to zero). Flow patterns were also observed by decreasing the air volumetric flux to examine if there was any hysteresis in them. A hi-vision video camera (SONY, HDR-FX1) and high speed camera (Redlake, HS-1) were used to record flow patterns.

2.2.2 CCFL characteristics

In the experiments, Q_{Lin} and J_G, were changed, and the relationships between J_L of the volumetric flux of the water flow into the lower tank and J_G were obtained. CCFL data were plotted on the Wallis diagram to fit them with the Wallis correlation (Wallis, 1969), which is the most widely used correlation for CCFL characteristics,

$$J_G^{*1/2} + mJ_L^{*1/2} = C \tag{1}$$

where m and C are empirical constants depending on fluid type and channel geometry. J_K* (k=G, L) is dimensionless flux and defined as follows.

$$J_k^* = J_k \left\{ \frac{\rho_k}{g \cdot D(\rho_L - \rho_G)} \right\}^{1/2}, \text{ (k=G,L)} \tag{2}$$

where ρ is density, g is gravity acceleration, and D is diameter of a pipe.

2.3 Experimental results of 1/5th rectangular duct

2.3.1 Flow patterns

Flow patterns could be classified into the following three regimes.

(A) Stratified flow

At low J_G, the gas and liquid phase was stratified in all sections of the hot leg. Few waves were observed in the horizontal section. **Figures 5-7** show typical images of the stratified flows in the horizontal, elbow and inclined sections, respectively. Injected water formed a thin water film at the bottom of the flow channel and sped up in the inclined and elbow sections. Water slowed down in the horizontal section and a hydraulic jump occurred due to the transition from supercritical flow to subcritical flow. The onset of a hydraulic jump in the flow channel depended on Q_{Lin} and J_G. At high J_G, the hydraulic jump appeared near the elbow. Under the stratified condition in this study, the hydraulic jump always appeared.

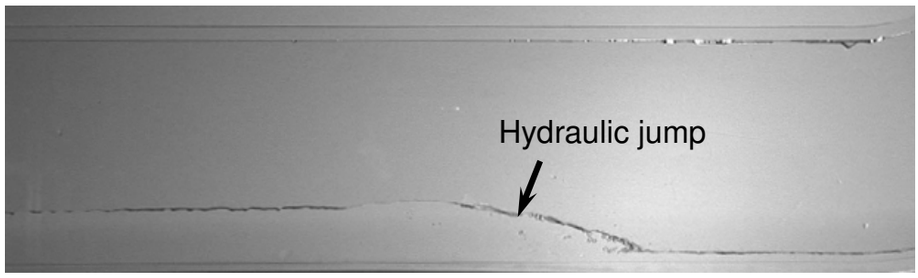

Fig. 5. Typical image of stratified flow in the horizontal section (Q_{Lin}=5 l/min, J_G=4.3 m/s)

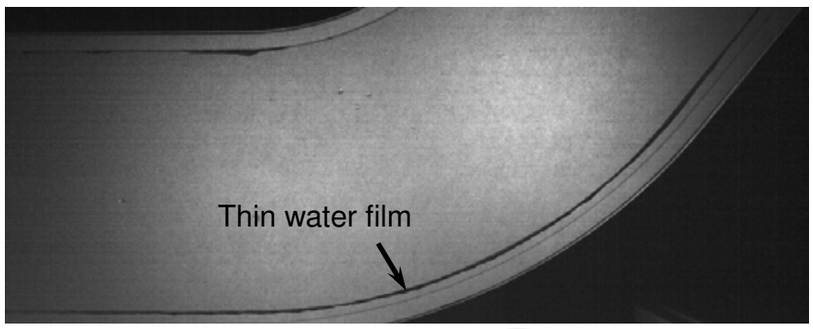

Fig. 6. Typical image of stratified flow in the elbow section (Q_{Lin}=5 l/min, J_G=4.3 m/s)

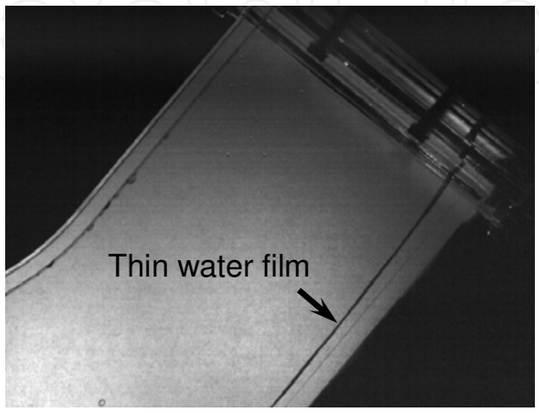

Fig. 7. Typical image of stratified flow in the inclined section (Q_{Lin}=5 l/min, J_G=4.3 m/s)

(B) Wavy flow

As J_G increased, the gas-liquid interface started to ruffle, and the flow pattern transited from stratified to wavy flow.

Figures 8(I) and (II) show images of wavy flows in the horizontal section. The onset point of wave depended on Q_{Lin}. At low Q_{Lin}, the wave appeared near the air inlet, then grew up and transferred toward the elbow section, as shown in Fig. 8(I). On the other hand, at high Q_{Lin}, an unstable interface formed in the horizontal section near the elbow, and disturbance wave occurred there, as shown in Fig. 8(II). Under the condition that the wavy flow formed in the horizontal section, the wavy flow also formed in the elbow section due to inflow of wave generated in the horizontal section. In the bottom region, a circulation flow of water with bubble and droplet formed. In the upper region of the elbow, it was stratified flow with a thin water film (in other words, the wavy flow was not observed in the inclined section).

Figure 9 shows the typical image of wavy flows in the elbow section.

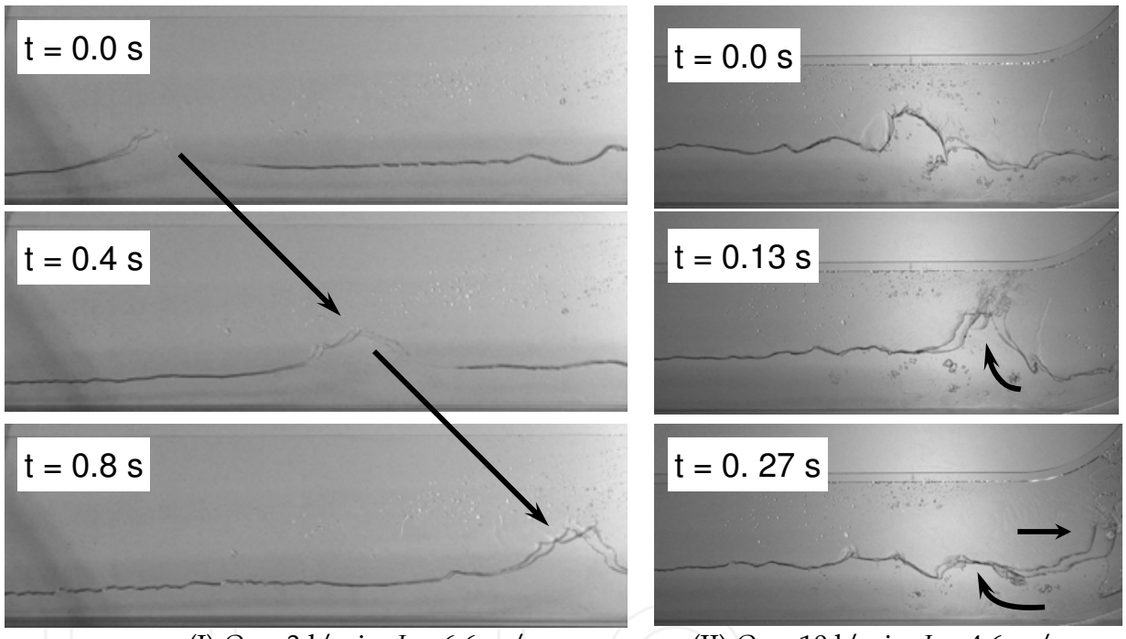

(I) Q_{Lin}=3 l/min, J_G =6.6 m/s (II) Q_{Lin}=10 l/min, J_G =4.6 m/s

Fig. 8. Typical images of wavy flow in the horizontal section

(C) Wavy-mist flow

With further increase in J_G, air velocity became high near the wave peak which finally broke up. Some injected water returned to the upper tank which overflowed. This flow pattern is referred to as wavy-mist flow. **Figure 10** shows a typical image of wavy-mist flow in the horizontal section. For wavy-mist flow, mist occurred at the elbow side while wavy flow occurred at the lower tank side. In the elbow and inclined sections, the wavy-mist flow also formed due to inflow of mist generated in the horizontal section. **Figures 11** and **12** show typical images of wavy-mist flow in the elbow and inclined sections, respectively. A circulation flow with large disturbance waves formed in the liquid phase when the large wave occurred in the horizontal section. The circulation flow with large disturbance waves involved bubbles in the water flow.

When J_G was more than 10.8 m/s, zero water penetration with no flow to the lower tank was achieved. At that time wavy-mist flow formed near the elbow, while wavy flow formed near the lower tank. In addition, a liquid phase leading edge moved to the elbow side with the increase in the air velocity. **Figure 13** shows a typical image.
When J_G was more than 21.3 m/s, no water was in the horizontal section, as shown in **Fig. 14**.

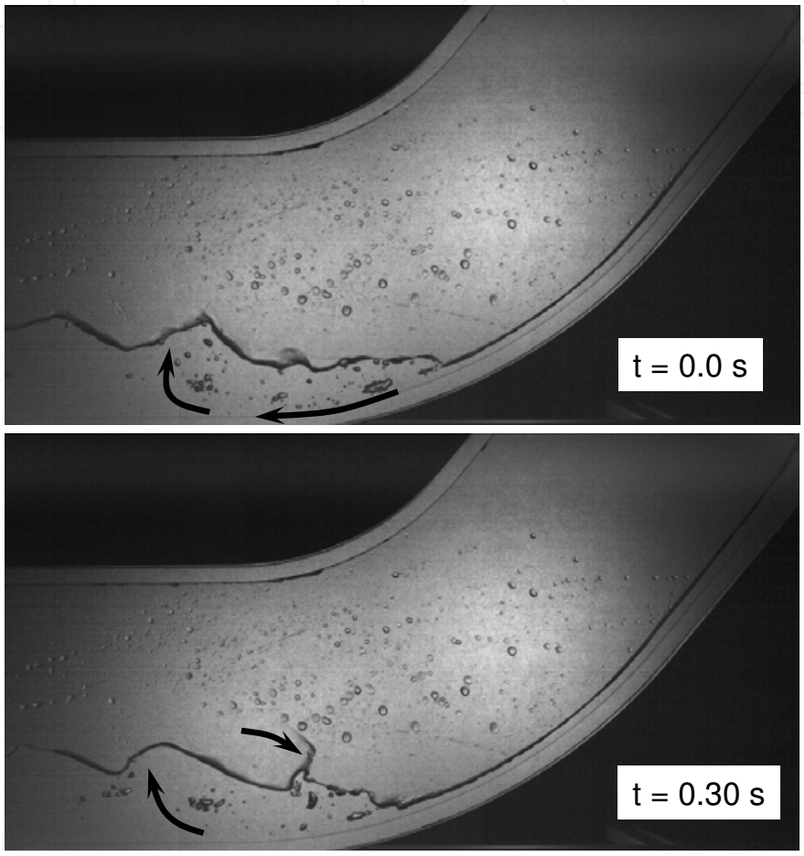

Fig. 9. Typical images of wavy flow in the elbow section (Q_{Lin}=5 l/min, J_G=6.3 m/s)

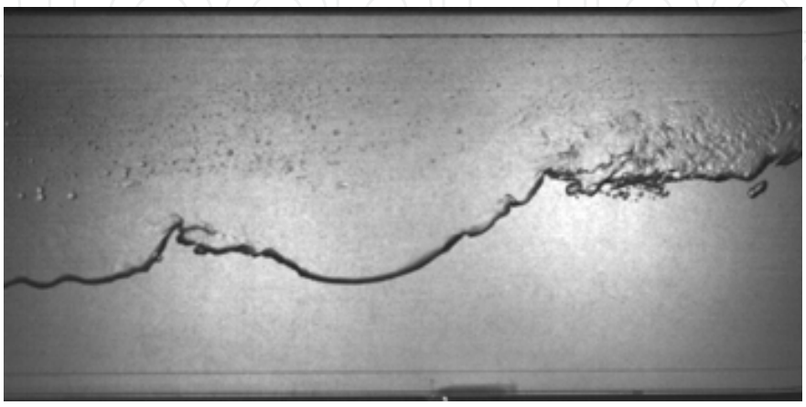

Fig. 10. Typical image of wavy-mist flow in the horizontal section (Q_{Lin}=5 l/min, J_G=9.0 m/s)

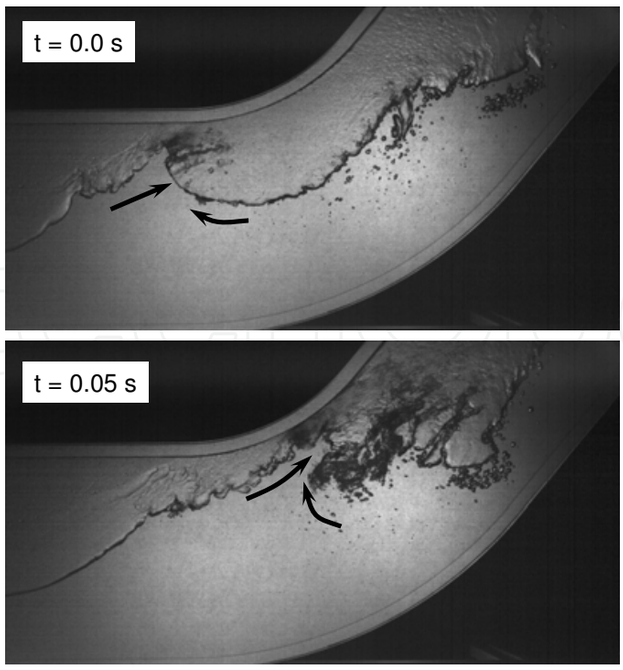

Fig. 11. Typical images of wavy-mist flow in the elbow section (Q_{Lin}=5 l/min, J_G=9.0 m/s)

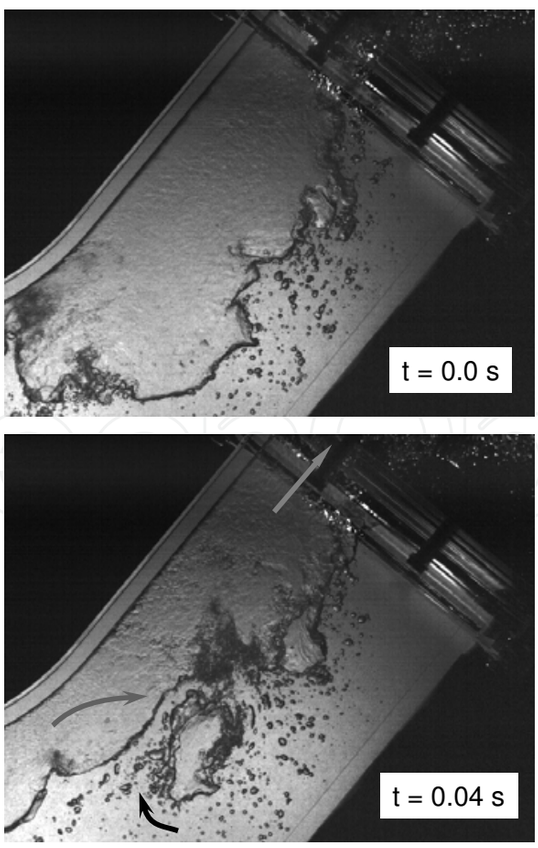

Fig. 12. Typical images of wavy-mist flow in the inclined section (Q_{Lin}=5 l/min, J_G=9.0 m/s)

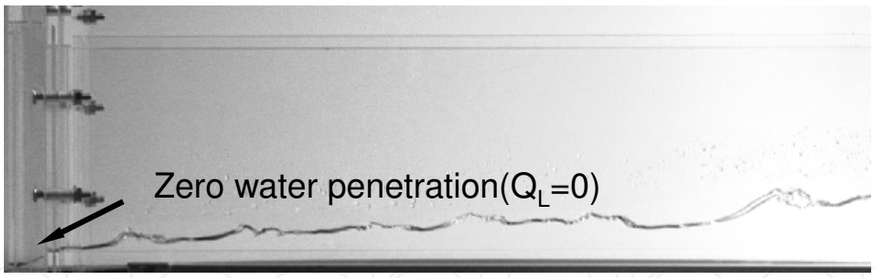

Fig. 13. Typical image of zero water penetration in the horizontal section (Q_{Lin}=5 l/min, J_G= 10.8 m/s)

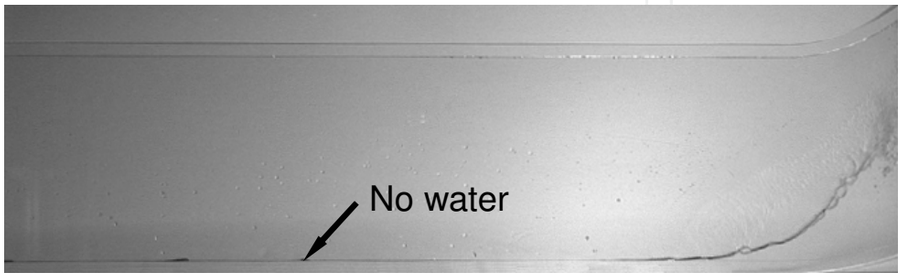

Fig. 14. Typical image of dry condition in the horizontal section (Q_{Lin}=5 l/min, J_G=21.3 m/s)

2.3.2 Flow pattern map

Figure 15 shows the flow pattern maps in the horizontal, elbow and inclined sections, respectively. In the horizontal section, as J_G increased for a given Q_{Lin}, the flow pattern changed from stratified flow to wavy flow, and then wavy to wavy-mist flow. After transition to wavy-mist flow, water flow into the lower tank through the horizontal section started to be restricted. Further increase in J_G caused zero water penetration at J_G=10.8 m/s and finally no water was present in the horizontal section for J_G>21.3 m/s. Flow pattern transition from stratified flow to wavy flow and wavy to wavy-mist flow occurred at low J_G condition when Q_{Lin} was large. This was because higher Q_{Lin} led to a large water depth and narrow air flow area, and local air velocity increased. On the other hand, J_G at the transition to zero water penetration did not depend on Q_{Lin}.

In the elbow section, as J_G increased, the transition to wavy flow began due to the intrusion of wavy flow generated in the horizontal section. Therefore, J_G at the transition was almost the same as that in the horizontal section. Further increase in J_G caused flow pattern transition to wavy-mist flow due to droplets breaking from the peaks of the waves.

In the inclined section, when water accumulated in the upper tank and overflow occurred, the flow pattern changed from stratified flow to wavy-mist flow without the appearance of wavy flow. Flow patterns in the elbow and inclined sections were strongly affected by those in the horizontal section.

2.3.3 CCFL characteristics

Figure 16 plots experimental results for the relationship between $J_G^{*0.5}$ and $J_L^{*0.5}$. In this figure, the duct height of this study was used for D in Eq. (2). There was a linear relationship between $J_G^{*0.5}$ and $J_L^{*0.5}$. CCFL characteristics did not depend on Q_{Lin}, and CCFL constants were m=0.67 and C=0.56 in Eq. (1).

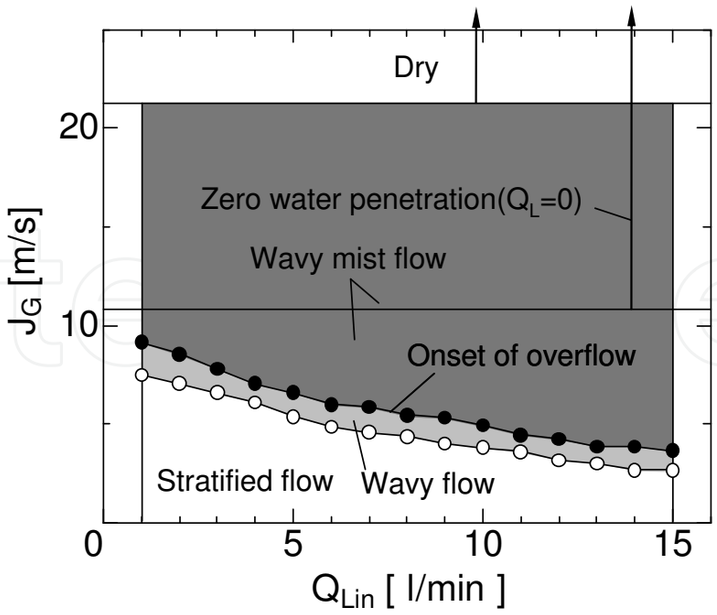

(a) Horizontal section

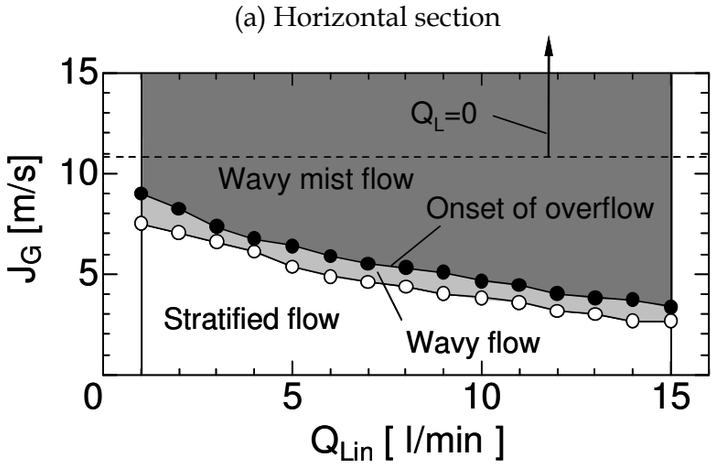

(b) Elbow section

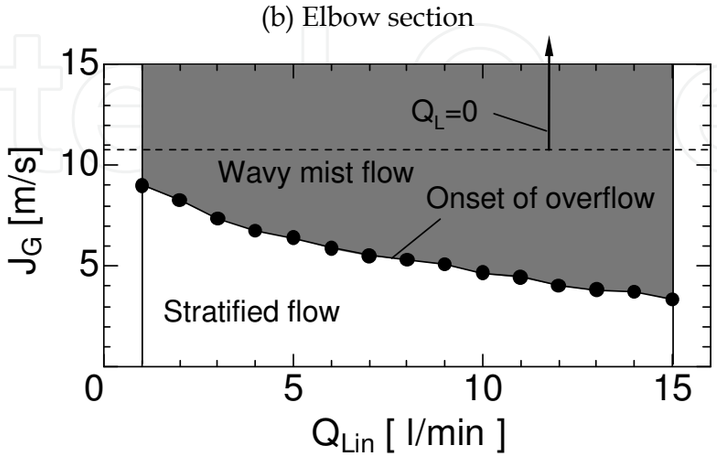

(c) Inclined section

Fig. 15. Flow pattern maps

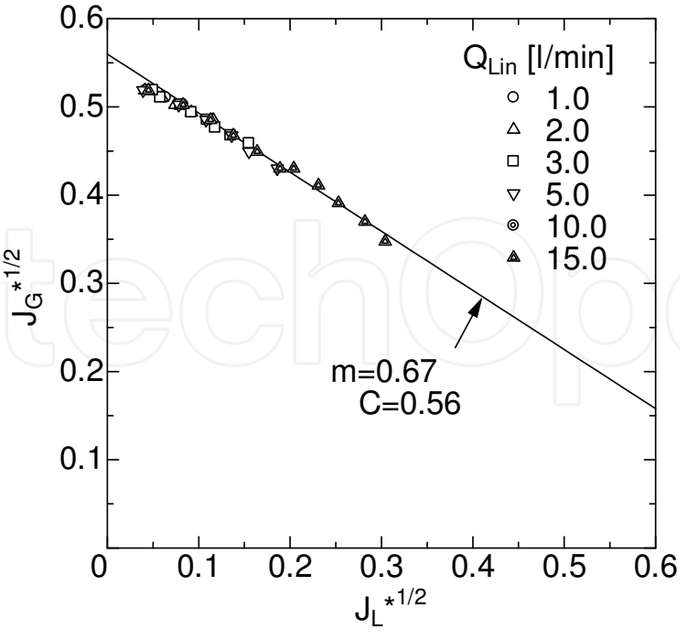

Fig. 16. CCFL characteristics

2.3.4 Relationship between CCFL characteristics and flow pattern transition

Figure 17 shows the relationship between CCFL characteristics and flow pattern transitions. The flow pattern transitioned from stratified to wavy flow and wavy to wavy-mist flow showed a linear relationship. The transition line from wavy flow to wavy-mist flow agreed well with the CCFL correlation.

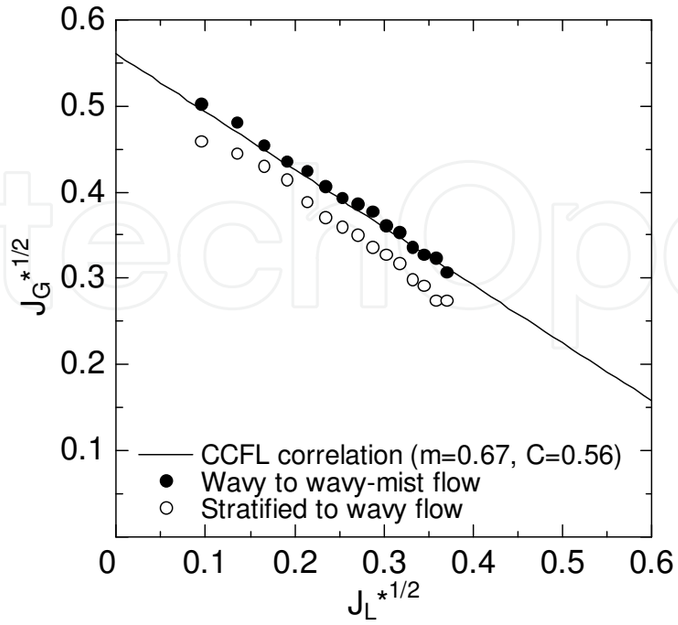

Fig. 17. Relationship between CCFL and flow pattern transitions

2.4 Experimental results of 1/15th circular pipe

2.4.1 Flow patterns

Flow patterns could be classified into the following four regimes.

(A) Stratified flow

At low J_G, the gas and liquid phases were separated in all sections of the hot leg as shown in **Fig. 18**. In this regime, supplied water was not limited and all the water flowed into the lower tank. The hydraulic jump observed in the rectangular test was not observed. This should be considered due to the water not being enough acceleration to achieve supercritical flow.

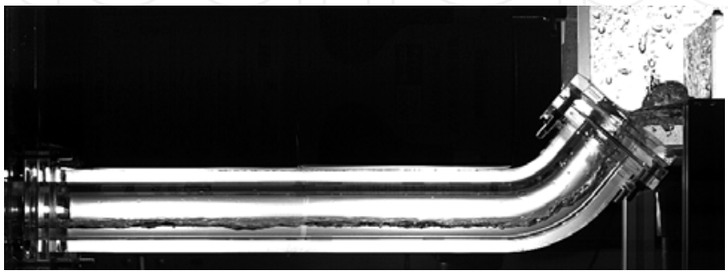

Fig. 18. Stratified flow Q_{Lin}=20 l/min, J_G=4.3 m/s (increasing J_G)

(B) Wavy(+) flow

As J_G increased, the supplied water accumulated in the upper tank and covered the junction of the hot leg and the upper tank. The air penetrated the liquid phase intermittently. Hence the gas-liquid interface fluctuated at the junction, and some of the supplied water flowed back into the reservoir, that is, CCFL took place at the upper end of the inclined section. In this condition, waves that formed in all sections of the hot leg were caused by this fluctuation. Taking the direction from the upper tank to the lower tank as the positive direction, then the sign of the wave velocity is positive. This flow pattern is referred to as wavy(+) flow. A typical image of this condition is shown in **Fig. 19**.

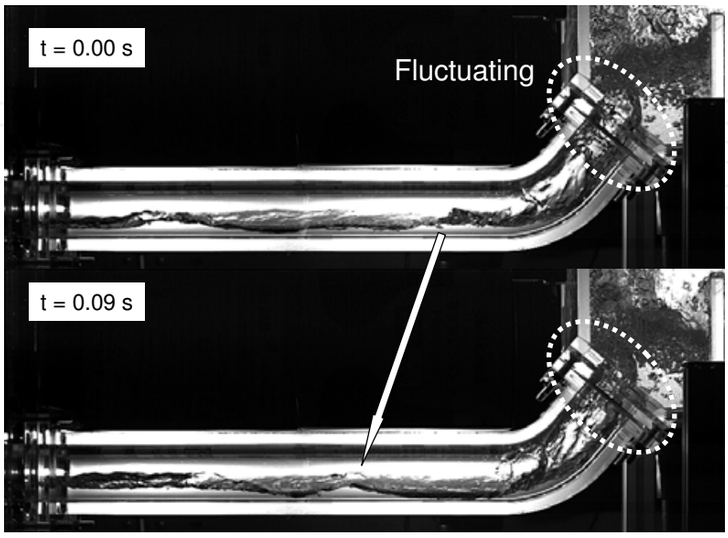

Fig. 19. Wavy(+) flow Q_{Lin}=20 l/min, J_G=4.8 m/s (increasing J_G)

(C) Wavy(-) flow

Further increase in J_G caused flow disturbance in the hot leg. When wave height was high, the flow pattern in the horizontal section immediately changed to wavy flow with a negative wave velocity. This flow pattern is referred to as wavy(-) flow. **Figure 20** shows a typical image. A mist occurred in the elbow side in the horizontal section. In the elbow and inclined section, annular-mist flow, in which the liquid phase reached the upper wall of the pipe and entrained upward, was observed. This was due to the intrusion of the waves with breaking of droplets generated in the horizontal section. Circulation of water with bubbles and droplets was formed. The flow in the elbow and the inclined section strongly fluctuated.

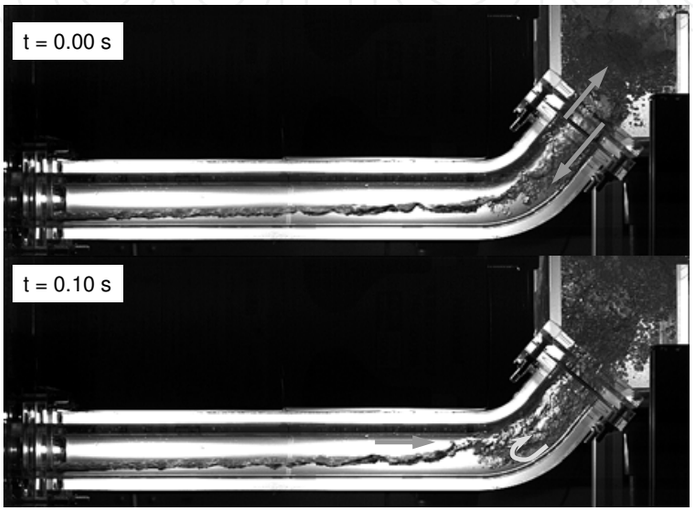

Fig. 20. Wavy(-) flow Q_{Lin}=20 l/min, J_G=6.5 m/s (increasing J_G)

(D) Oscillatory flow

As J_G decreased from the negative wavy flow condition, the injected air did not penetrate the liquid phase in the upper tank and oscillatory flow (**Fig. 21**) was observed. The flow patterns in the elbow and the inclined section were also oscillatory flow.

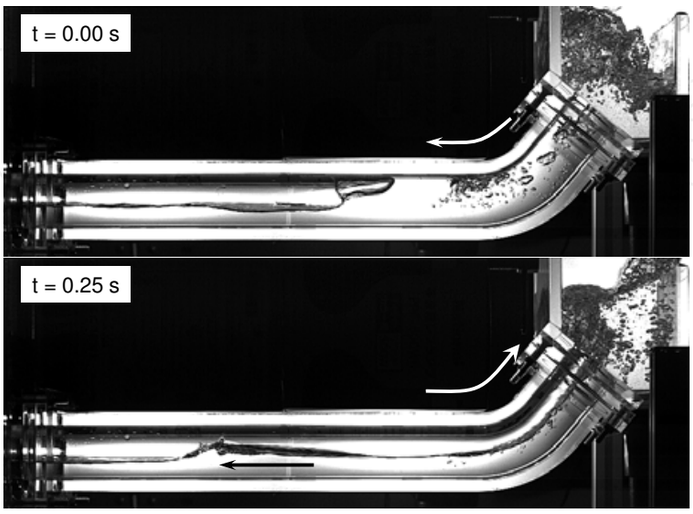

Fig. 21. Oscillatory flow Q_{Lin}=20 l/min, J_G=0.65 m/s (decreasing J_G)

2.4.2 Flow pattern map

Flow pattern maps obtained by increasing J_G and decreasing J_G are shown in **Figs. 22(a)** and **(b)**, respectively. There was a large difference in the two maps. When Q_{Lin} was high ($\geq$ 15 l/min), the junction of the hot leg and the upper tank was covered with the air-water mixture as J_G increased. Thus the flow pattern transited from stratified flow to wavy(+) flow. Further increase in J_G caused the flow pattern transition to wavy(-) flow in the horizontal section. On the other hand, when Q_{Lin} was low (< 15 l/min), air and water were separated at the junction of the hot leg and the upper tank. Hence the stratified flow was kept for J_G < 8 m/s. At J_G = 8 m/s, the flow pattern directly transited from stratified flow to wavy(-) flow in the horizontal section and to annular-mist flow in the elbow and inclined section.

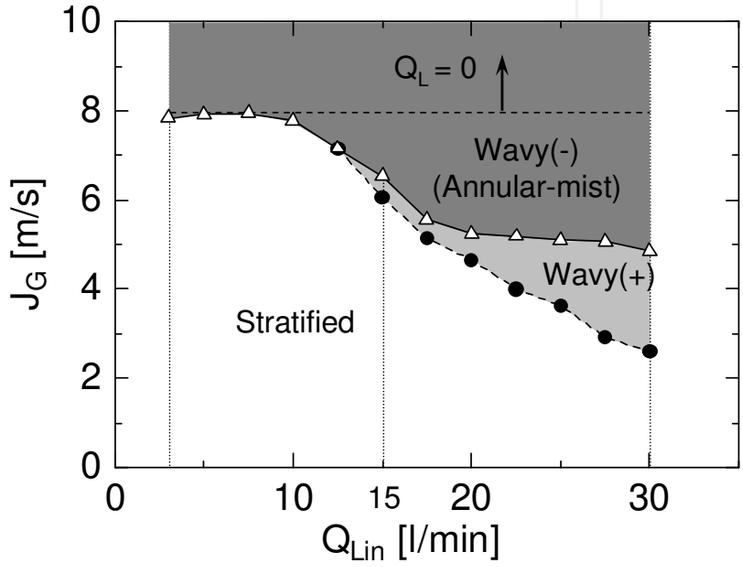

(a) Increasing J_G

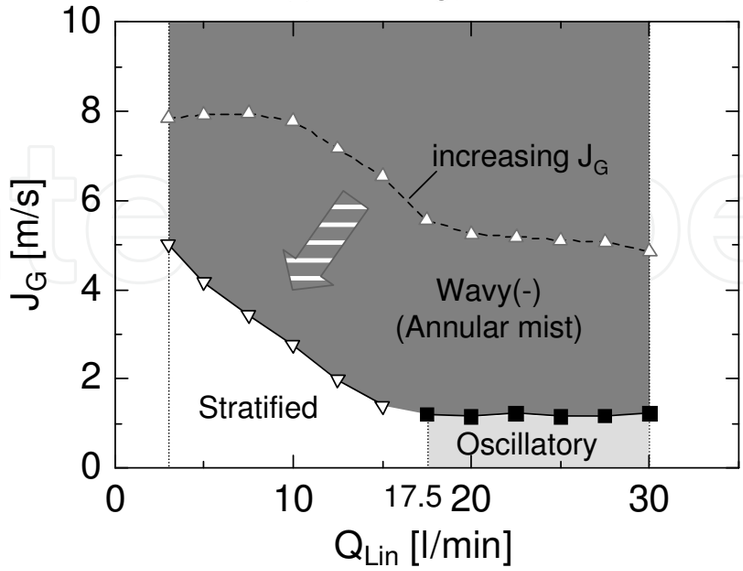

(b) Decreasing J_G

Fig. 22. Flow pattern maps

In this condition, water ceased to flow into the lower tank. The flow pattern transition to annular-mist flow took place simultaneously with the flow pattern transition to wavy(-) flow in the horizontal section. This was due to the intrusion of waves generated in the horizontal section into the elbow. Flow patterns in the elbow and the inclined section were, therefore, strongly affected by those in the horizontal section. The transition from wavy(-) to stratified flows when decreasing J_G took place at a lower J_G than the transition from stratified to wavy flows when increasing J_G. That is, there was a hysteresis in the flow pattern transition. In the case of $Q_{Lin} \geq 17.5$ l/min, the flow pattern in the whole hot leg transited to oscillatory flow as J_G decreased. It should be noted that (a) the amount of water accumulation in the upper tank has nothing to do with the hysteresis appearing in the hot leg, and (b) the same kind of hysteresis in flow patterns has also been observed in countercurrent flows in a vertical pipe (Hewitt & Wallis, 1963).

2.4.3 CCFL characteristics

Figure 23(a) shows the CCFL characteristics at Q_{Lin} = 10, 20 and 30 l/min. The CCFL characteristics obtained by increasing J_G^* differed from those obtained by decreasing J_G^*. In the case of Q_{Lin} = 20 l/min (as the base case), as J_G gradually increased, CCFL first occurred at the upper end of the inclined section and the flow pattern transited to wavy(+) flow. As J_G^* increased, the flow pattern in the horizontal section transited from wavy(+) to wavy(-) flows. In this condition, CCFL occurred in the horizontal section. When this transition occurred, J_L^* decreased abruptly by a slight increase in J_G^*. When the water height was high due to overlapping of these waves, waves were pushed back toward the upward direction (Fig. 23(b)), and the flow pattern transited to wavy(-) flow.

When J_G^* decreased, the flow remained as wavy(-) flow. When the flow pattern in the horizontal section was wavy(-) flow, CCFL characteristics showed a linear relationship. Though the values of $J_G^{*1/2}$ in Figs. 23(a)(I) and (II) were the same, the flow in (II) was more restricted than that in (I). This was due to the difference in the flow pattern in the horizontal section. Hence, the CCFL characteristics were closely related with the flow patterns.

In the case of Q_{Lin} = 10 l/min, as J_G increased, the flow pattern in the horizontal section suddenly transited from stratified to wavy flow. A typical image of this transition is shown in Fig. 23(c). This transition was due to the wave generated in the gas inlet. In this case, wavy(+) flow did not appear because the water did not cover the junction at any J_G. After this transition, no water flowed into the lower tank at $J_G^{*1/2}$ = 0.62. The CCFL characteristics obtained by decreasing J_G agreed well with those in the case of Q_{Lin} = 20 l/min.

In the case of Q_{Lin} = 30 l/min, the junction of the hot leg and the upper tank was covered with the supplied water at $J_G^{*1/2}$= 0. For $J_G^{*1/2} \geq 0.3$, CCFL took place at the upper end of the inclined section, for which the CCFL characteristics followed the linear relationship between $J_G^{*1/2}$ and $J_L^{*1/2}$. $J_G^{*1/2}$ was decreased from 0.6 to 0.2, the flow pattern in the horizontal section was wavy(-) flow and the CCFL characteristics agreed well with those in the case of Q_{Lin} = 20. For $J_G^* < 0.2$, the flow pattern in the horizontal section transited from wavy(-) to oscillatory flow, and the CCFL characteristics at $J_G^{*1/2}$ = 0.16 disagreed with the Wallis correlation.

The CCFL characteristics obtained by increasing J_G depended on Q_{Lin}. This was because CCFL at the junction was affected by the water level in the upper tank which depends on Q_{Lin}. It should be noted that the water level in the upper tank might relate to the dimensions of the inlet plenum of the upper tank. On the other hand, the CCFL characteristics obtained

by decreasing J_G did not depend on Q_{Lin}. This was because CCFL occurred at the horizontal section and it depended not on Q_{Lin} but on J_L.

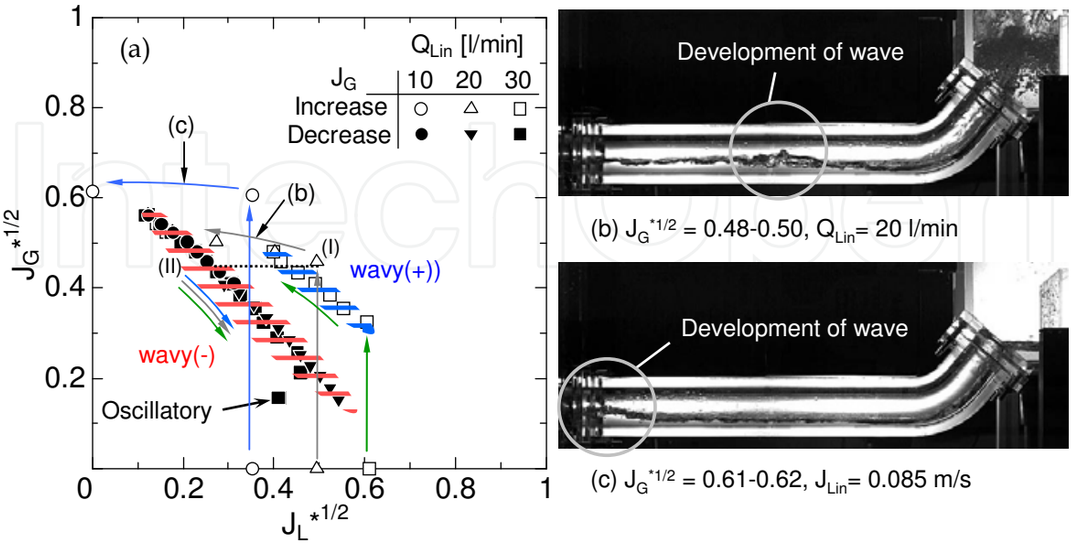

Fig. 23. Relationship between CCFL characteristics and flow patterns

Figure 24 shows CCFL characteristics in the case with decreasing J_G. The boundary between wavy(-) flow and stratified flow agreed well with the CCFL characteristics. This result indicated that CCFL characteristics were closely related with the flow patterns in the hot leg and that the onset of deflooding or the flow pattern transition line agreed with the CCFL line.

Figure 24 also compares CCFL data in the literature (Ohnuki, 1986, Mayinger et al., 1993) and the present study. Ohnuki (1986) examined the countercurrent flow using air-water and saturated steam-water systems with a 0.6 m length 45° inclined pipe and a 0.3 m length horizontal pipe with the inner diameter of 0.051 m, and a 0.6 m length 45° inclined pipe and a 0.4 m length horizontal pipe with the inner diameter of 0.076 m, in order to investigate the effects of length-to-diameter ratio in the horizontal pipe, the shape of the upper exit of the inclined riser, and the length of the inclined riser. Mayinger (1993) used a full-scale apparatus simulating the hot leg. Test conditions in these studies are summarized in Table 1. Though all the hot legs were of different sizes and fluid properties, these data were very close together.

		Inner diameter[m]	Length of the horizontal section [m]	Angle of elbow [deg]	Working fluid
This study		0.050	0.43	50	Air-water
Mayinger et al.(1993)		0.75	7.20	50	Steam-water
Ohnuki (1986)	(1)	0.051	0.30	45	Air-water
	(2)	0.051	0.30	45	Steam-water
	(3)	0.076	0.40	45	Air-water
	(4)	0.076	0.40	45	Steam-water

Table 1. Test conditions

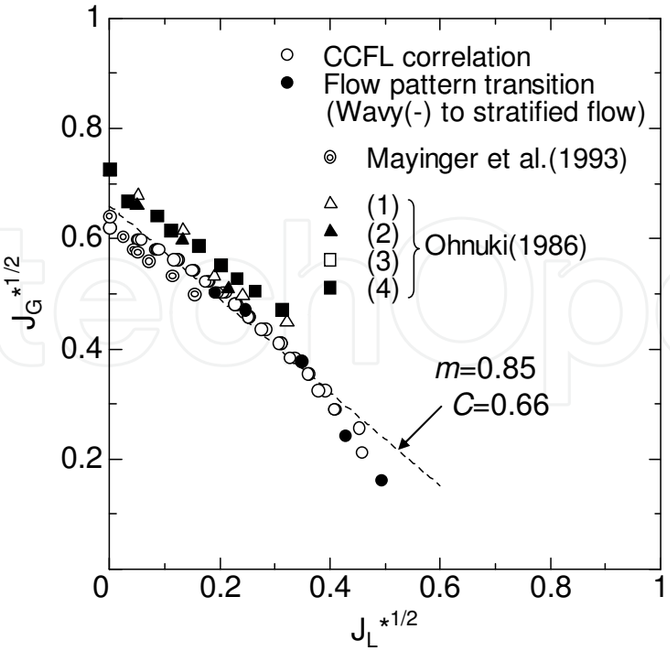

Fig. 24. Comparison with previous CCFL data

3. Numerical calculations

We carried out three-dimensional calculations of the scale model of the PWR hot legs mentioned in section 2 to examine the feasibility of predicting these complicated flow patterns and CCFL characteristics in the hot leg using a standard two-fluid model.

3.1 Numerical method

In numerical calculations, we adopted the two-fluid model and the k-ε model in the CFD code, FLUENT6.3.26. Correlations for interfacial friction coefficients are required when applying the code to a two-phase flow of concern. The interfacial friction force $\boldsymbol{F}_i$ in the momentum equation is defined by:

$$\boldsymbol{F}_i = \frac{1}{2} C_D a_i \rho_G |\boldsymbol{u}_r| \boldsymbol{u}_r \,, \tag{3}$$

where $\boldsymbol{u}_r$ is the relative velocity between the gas and liquid phases, and a_i is the interfacial area concentration. The interfacial friction coefficient, $C_D a_i$, applicable to three-dimensional simulations has not been established. We therefore tested various combinations of correlations developed for a one-dimensional two-fluid model. Then we selected a combination of correlations which gave the best agreement with the experiments. The resulting combination is given by

$$C_D a_i = min\left[\left(C_D a_i\right)_B, max\left\{ \left(C_D a_i\right)_S, \left(C_D a_i\right)_A \right\} \right], \tag{4}$$

$$\left(C_D a_i\right)_B = 2\alpha(1-\alpha) g / V_{GJ}^2 \,, \tag{5}$$

$$\left(C_D a_i\right)_S = 9.8\left(1-\alpha\right)^3\left(\frac{4.5\alpha}{D_h}\right), \tag{6}$$

$$\left(C_D a_i\right)_A = 0.02\left\{1+75\left(1-\alpha\right)\right\}\alpha^{0.5} / D_h, \tag{7}$$

where α is the void fraction, V_{GJ} is the drift velocity of the gas phase and D_h is the hydraulic diameter. Equations (5), (6) and (7) are for low (Minato et al., 2000), intermediate (Ishii & Mishima, 1984) and high (Wallis, 1969) void fraction regions, respectively. The drift velocity is given by (Kataoka et al., 1987):

$$V_{GJ} = \left\{1.4-0.4\,exp\left(-10\alpha\right)\right\}\left(D_h^*\right)^{0.125}\left\{\frac{g\sigma\left(\rho_L-\rho_G\right)}{\rho_L^2}\right\}^{1/4} \tag{8}$$

where

$$D_h^* = D_h\left\{\frac{g\left(\rho_L-\rho_G\right)}{\sigma}\right\}^{1/2}, \tag{9}$$

and σ is the surface tension. The following simplified form of Eq. (8) was used in the present simulations:

$$V_{GJ} = 1.4\left(D_h^*\right)^{0.125}\left\{\frac{g\sigma\left(\rho_L-\rho_G\right)}{\rho_L^2}\right\}^{1/4}. \tag{10}$$

3.2 Computational grid

We carried out three-dimensional simulations using a computational domain including the lower and upper tanks to avoid uncertainties in the inlet and outlet boundary conditions and to accurately evaluate the wall friction.

3.2.1 1/5th-scale rectangular duct

Figure 25 shows the computational grid. Air was supplied into the lower tank through the air-inlet pipe at a constant velocity. Water was supplied from the bottom of the upper tank at a constant velocity. J_L was calculated from the increasing rate of the mass of water in the lower tank. When CCFL occurred in the hot leg, some water overflowed the upper tank and flowed out through the mixture outlet. The pressure at the mixture outlet was set constant.
The hot leg was a rectangular cross section (10 mm wide and 150 mm high). The height was about 1/5th of the pipe diameter of an actual PWR hot leg. The inclination of the inclined pipe was 50°. The geometry was the same as the experiment for the rectangular duct. Hence the total number of cells was about 140,000.

3.2.2 1/15th-scale circular pipe

Figure 26 shows the computational grid. The size was the same as that of the 1/15-scale model. Air was supplied into the lower tank through the air-inlet pipe at a constant velocity. Water was supplied from the bottom of the upper tank at a constant velocity. Unlike the tests, water was supplied from all over the bottom to minimize external influence.

Calculations were done for Q_{Lin} = 10- 30 l/min. The air velocity was increased until J_L = 0 and decreased. The total number of cells was about 70,000 except Q_{Lin} = 10 l/min. There was a possibility that the flow in the hot leg was not simulated faithfully due to the rough size of the simulation cells, especially where the water depth was shallow. This was because the sizes of cells affected simulations of water accumulation at the gas inlet. Hence, we used the fine mesh at Q_{Lin} = 10 l/min and the total number of cells was about 120,000.

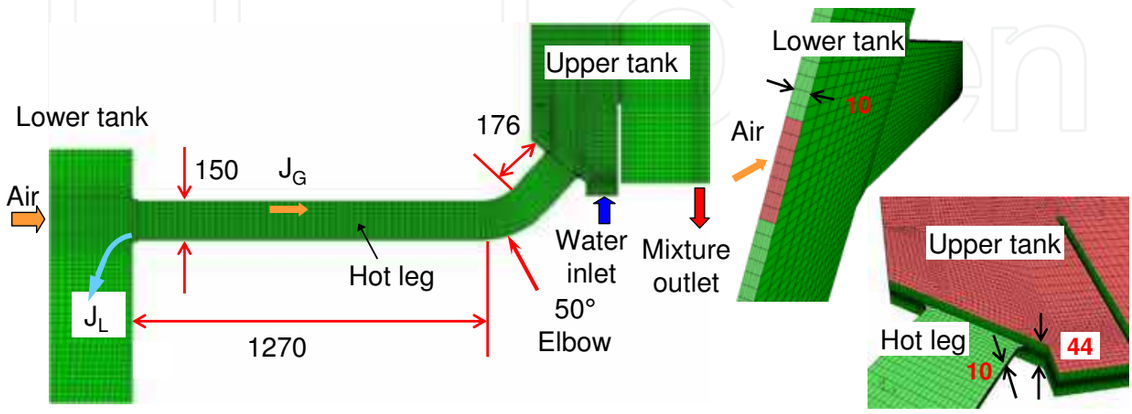

Fig. 25. Computational grid with 1/5th-scale rectangular pipe (unit: mm)

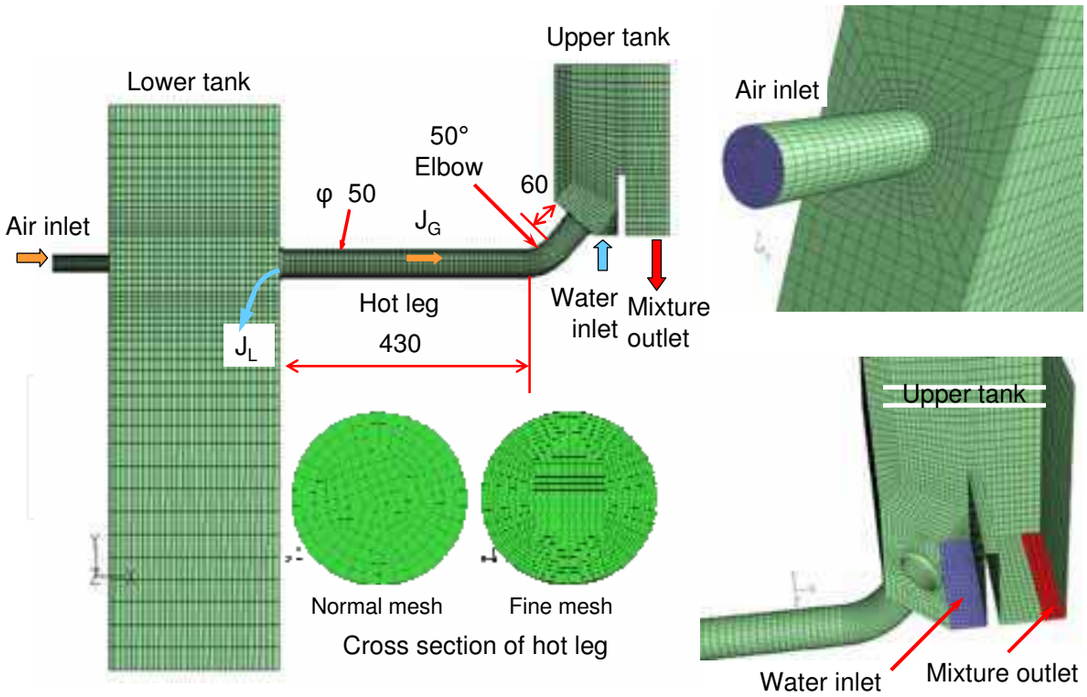

Fig. 26. Computational grid with 1/15th-scale circular pipe (unit : mm)

3.3 Calculation results

3.3.1 1/5th-scale rectangular duct

The aim of this calculation was to predict the wavy-mist flow observed in the experiments.

Figure 27 shows the predicted flow pattern after achieving the quasi-steady state. Flooding occurred in the hot leg. The liquid phase dropped from the upper tank and accumulated near the elbow in the horizontal section. Then the wave formed and was blown up to the upper tank. The predicted flow pattern could reproduce the wavy-mist flow in the experiments. To predict the flow pattern in the experiment, it is important to simulate the hot leg including the upper tank and the lower tank faithfully.

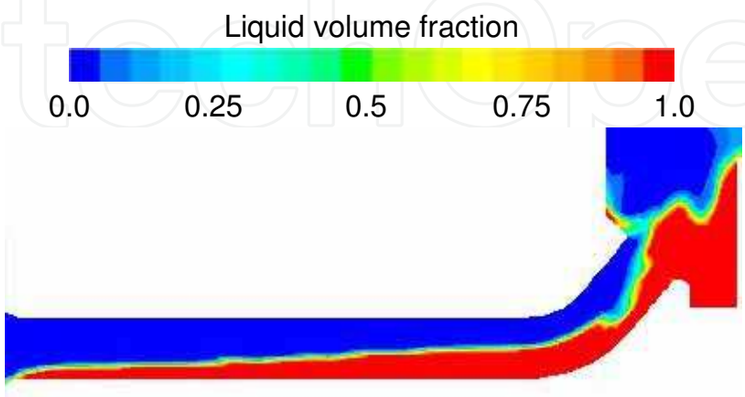

Fig. 27. Predicted flow pattern (Q_{Lin} = 36 l/min, J_G = 9.5 m/s)

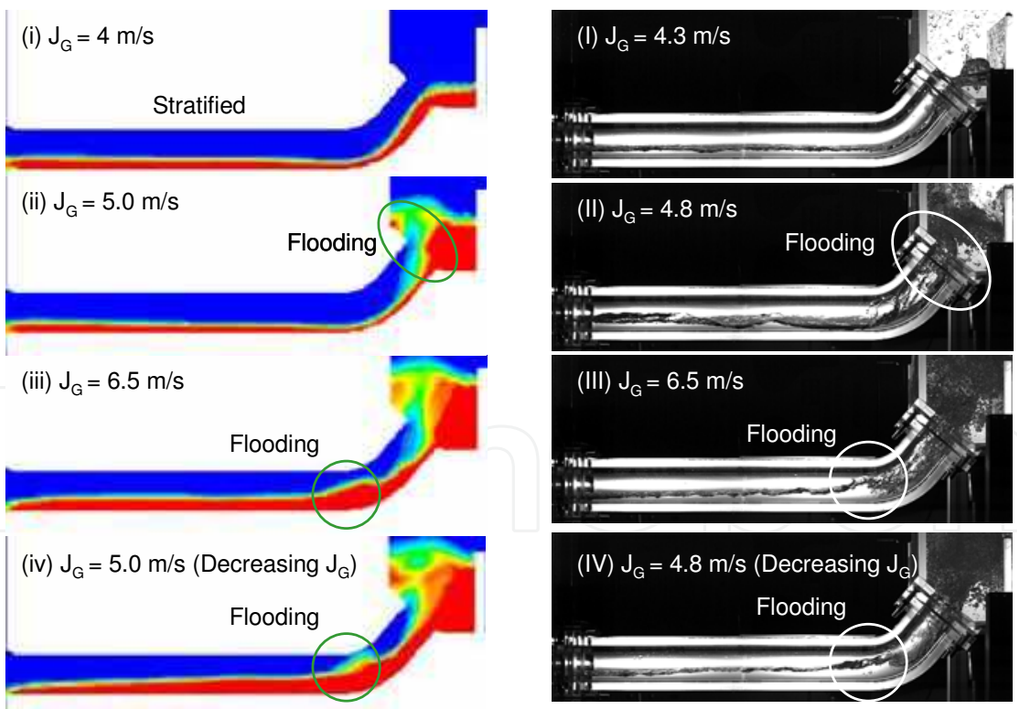

Fig. 28. Comparison between the predicted and measured flow patterns (Q_{Lin} = 20 l/min)

3.3.2 1/15th-scale circular pipe

Figure 28 compares predicted and measured flow patterns at Q_{Lin} = 20 l/min. In the simulation, at low J_G , a stratified flow was calculated in all sections of the hot leg as shown

in (i). As J_G increased, fluctuation of flow took place at the junction of the hot leg and the upper tank as shown in (ii). At J_G = 6.5 m/s as shown in (iii), the flow pattern near the elbow in the horizontal section was a wavy flow, whereas it was a wavy-mist flow in the elbow and the inclined section. When we decreased J_G from 6.5 m/s, the flow pattern remained unchanged even though J_G was the same as in (ii). These flow behaviors were almost the same as the observed flow patterns as shown in (I) to (IV).

Figure 29 shows a comparison between calculated and measured CCFL characteristics at Q_{Lin} = 10, 20 and 30 l/min. At Q_{Lin} = 10, 20 l/min, the calculated CCFL characteristics agreed well with the measured data. On the other hand, at Q_{Lin} = 30 l/min, J_L* in the simulation resulted in underestimation of J_L* in the test at low J_G*. This was due to a large difference between the measured and the predicted flow patterns at the junction of the hot leg and the upper tank. In the simulation, the flow was calm, whereas the flow fluctuated at the junction as shown for the measured data (Fig. 29(b)).

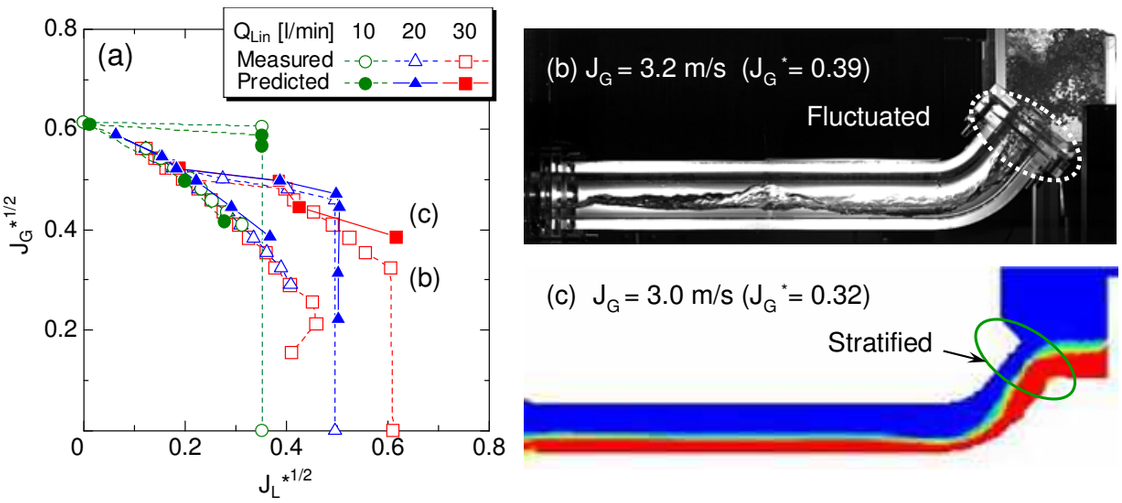

Fig. 29. Comparison between the calculated and measured CCFL data.

4. Conclusions

The objectives of this study were to clarify the flow patterns and dominant factors of countercurrent flow and to develop the flow model which improves the reliability of transient analysis. Results of experiments and numerical simulations for countercurrent flow in a PWR hot leg under reflux condensation were summarized, and the following conclusions were obtained.

i. The effects of gas and water flow rate on the flow patterns in the hot leg were clarified. Flow patterns in the elbow and the inclined section were strongly affected by those in the horizontal section.
ii. The flow patterns were closely related to the CCFL characteristics.
iii. The calculation results of scale model experiments agreed well with the measured data using an appropriate set of correlations for interfacial friction coefficient.

The combination of calculation model and interfacial friction coefficients used in this study can predict the countercurrent flow in a hot leg qualitatively and quantitatively.

5. References

Hewitt, G. F. & Wallis, G. B. (1963). ASME Multi-phase Flow Symposium, 62, Philadelphia, PA.

Ishii, M. & Mishima, K. (1984). Two-Fluid Model and Hydro-dynamic Constitutive Relations. *Nuclear Engineering and Design*, Vol. 82, 107-126.

Kataoka, Y. H. Suzuki & Murase, M (1987). Drift-Flux Parameters for Upward Gas Flow in Stagnant Liquid. *Journal of Nuclear Science and Technology*, Vol. 24 (7), 580-586.

Mayinger, F.; Weiss P. & Wolfert, K. (1993). Two-phase flow phenomena in full-scale reactor geometry. *Nuclear Engineering and Design*, Vol. 145, pp. 47-61.

Minami, N.; Nishiwaki, D.; Kataoka, H.; Tomiyama, A.; Hosokawa, S. & Murase, M. (2008a). Countercurrent Gas-Liquid Flow in a Rectangular Channel Simulating a PWR Hot Leg (1) Flow Pattern and CCFL Characteristics. *Japanese J. of Multiphase Flow*, Vol. 22, (4), pp. 403-412. (in Japanese)

Minami, N.; Murase, M.; Nishiwaki, D. & Tomiyama, A. (2008b). Countercurrent Gas-Liquid Flow in a Rectangular Channel Simulating a PWR Hot Leg (2) Analytical Evaluation of Countercurrent Flow Limitation. *Japanese J. of Multiphase Flow*, Vol. 22(4), pp. 413-422 (in Japanese).

Minami, N.; Nishiwaki, D.; Nariai, T.; Tomiyama, A. & Murase, M. (2010a). Countercurrent Gas-Liquid Flow in a PWR Hot Leg under Reflux Cooling (I), Air-Water Test for 1/15-Scale Model of a PWR Hot Leg, *Journal of Nuclear Science and Technology*, 47 [2], pp. 142-148.

Minami, N.; Murase, M. & Tomiyama, A. (2010b). Countercurrent Gas-Liquid Flow in a PWR Hot Leg under Reflux Cooling (II), Numerical Simulation for 1/15-Scale Air-Water Tests. *Journal of Nuclear Science and Technology*, 47 [2] pp. 149-155.

Minato, A.; Takamori, T. & Ishida, N. (2000). An Extended Two-Fluid Model for Interface Behavior in Gas-Liquid Two-Phase Flow. *Proc. of 8th Int. Conf. on Nuclear Engineering*, No. 8045 Baltimore, MD.

Navarro, M. A. (2005). Study of countercurrent flow limitation in a horizontal pipe connected to an inclined one. *Nuclear Engineering and Design*, Vol. 235, 1139-1148.

Ohnuki, A. (1986). Experimental Study of Counter-Current Two-Phase Flow in Horizontal Tube connected to an Inclined Riser. *Journal of Nuclear Science Technology*, Vol. 23 (3), pp. 219-232.

Ohnuki, A.; Adachi. H. & Murao, Y. (1988). Scale Effects on Countercurrent Gas-Liquid Flow in a Horizontal Tube Connected to an Inclined Riser. *Nuclear Engineering and Design*, Vol. 107, pp. 283-294.

Richter, H. J., et al., (1978), Deentrainment and Countercurrent Air-water Flow in a Model PWR Hot-leg, NRC-0193-9.

USNRC, (1987). *Loss of Residual Heat Removal System, Diablo Canyon, Unit 2 on April 10, 1987*, NUREG-1269, U. S. Nuclear Regulatory Commission.

USNRC, (1990). *Loss of Vital AC Power and the Residual Heat Removal System during Mid-Loop Operations at Vogtle Unit 1 on March 20, 1990*, NUREG-1410, U. S. Nuclear Regulatory Commission.

Wallis, G. B. (1969). One-dimensional Two-phase Flow, McGraw-Hill, New York.

Wongwises, S. (1996). Two-phase countercurrent flow in a model of a pressurized water reactor hot leg. *Nuclear Engineering and Design*, Vol. 166, pp. 121-133.

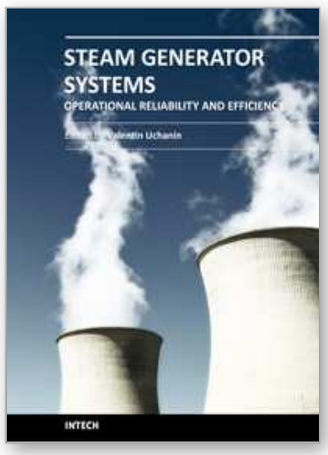

Steam Generator Systems: Operational Reliability and Efficiency
Edited by Dr. Valentin Uchanin

ISBN 978-953-307-303-3
Hard cover, 424 pages
Publisher InTech
Published online 16, March, 2011
Published in print edition March, 2011

The book is intended for practical engineers, researchers, students and other people dealing with the reviewed problems. We hope that the presented book will be beneficial to all readers and initiate further inquiry and development with aspiration for better future. The authors from different countries all over the world (Germany, France, Italy, Japan, Slovenia, Indonesia, Belgium, Romania, Lithuania, Russia, Spain, Sweden, Korea and Ukraine) prepared chapters for this book. Such a broad geography indicates a high significance of considered subjects.

How to reference
In order to correctly reference this scholarly work, feel free to copy and paste the following:

Noritoshi Minami, Michio Murase and Akio Tomiyama (2011). Countercurrent Flow in a PWR Hot Leg under Reflux Condensation, Steam Generator Systems: Operational Reliability and Efficiency, Dr. Valentin Uchanin (Ed.), ISBN: 978-953-307-303-3, InTech, Available from: http://www.intechopen.com/books/steam-generator-systems-operational-reliability-and-efficiency/countercurrent-flow-in-a-pwr-hot-leg-under-reflux-condensation

INTECH
open science | open minds

InTech Europe
University Campus STeP Ri
Slavka Krautzeka 83/A
51000 Rijeka, Croatia
Phone: +385 (51) 770 447
Fax: +385 (51) 686 166
www.intechopen.com

InTech China
Unit 405, Office Block, Hotel Equatorial Shanghai
No.65, Yan An Road (West), Shanghai, 200040, China
中国上海市延安西路65号上海国际贵都大饭店办公楼405单元
Phone: +86-21-62489820
Fax: +86-21-62489821

IntechOpen